Processing and Application of Ceramics 12 [4] (2018) 303–312
https://doi.org/10.2298/PAC1804303D

Microstructure evolution and dielectric properties of Ce-doped $SrBi_4Ti_4O_{15}$ ceramics synthesized via glycine-nitrate process

Huiling Du*, Cuiying Ma, Wuxiang Ma, Haiting Wang

School of Materials Science and Engineering, Xi'an University of Science and Technology, Xi'an, PR China

Received 18 April 2018; Received in revised form 20 August 2018; Accepted 22 October 2018

Abstract

Ce-doped strontium bismuth titanate ($SrBi_4Ti_4O_{15}$, SBT) powders were prepared by glycine-nitrate process at 400–500 °C and the ceramics were sintered at 980 °C. The phase composition, morphology and electric properties were investigated. It was found that the calcined powders consist of a single phase SBT and the calcination temperature is lower than that for the conventional solid state method. The morphology of Ce-doped SBT is flake-like and the layer size decreases with Ce-addition from 12 to 2 μm confirming that the addition of Ce^{3+} inhibits grain growth. The Curie temperature of Ce-doped SBT increased for about 20 °C compared to the pure SBT. The tan δ was ~0.005 at 35 °C and even below 0.05 up to 400 °C. The temperature coefficient of dielectric constant was ~0.012 and the rate of frequency change was 0.01–0.04, which indicated the high stability of dielectric properties of the Ce-doped SBT. Impedance analysis revealed that the conduction mechanism of the Ce-doped $SrBi_4Ti_4O_{15}$ ceramics is mainly grain conduction.

Keywords: *$SrBi_4Ti_4O_{15}$, Ce-doping, glycine-nitrate process, dielectric properties*

I. Introduction

Bismuth layer structured ferroelectrics (BLSFs), one of the lead-free piezoelectric ceramics, present good fatigue resistance properties, relatively high Curie point (T_c), and lead-free environmental friendly. They are applied widely in electronic devices like high temperature piezoelectric devices and non-volatile memories to replace traditional lead-based ceramics [1]. BLSF has a unique crystal structure where the bismuth oxide $(Bi_2O_2)^{2+}$ layers and pseudo perovskite $(A_{m-1}B_mO_{3m+1})^{2-}$ blocks stack alternately along their *c*-direction, where A represents a mono-, di- or trivalent ion or a mixture of them at a 12-coordinated site, B represents either a tetra-, penta- or hexavalent ion at a 6-coordinated site and *m* is the number (m = 1, 2, 3, 4 or 5) of BO_6 octahedras in a pseudo perovskite block [2].

The orthorhombic $SrBi_4Ti_4O_{15}$ (SBT), as a single-phase layered perovskite, is characterized by its high Curie temperature (T_c ~ 520 °C), low dielectric loss, high dielectric breakdown strength, high anisotropy and excellent fatigue endurance. It has attracted much of attention due to its promising applications in high temperature piezoelectric devices and high-density capacitors [3]. However, certain problems associated with SBT such as high leakage, difficulty in polarization, volatilization of the bismuth during sintering, and the random arrangement of plate-like crystal grains will lead to a low density and undesirable properties [4]. To overcome these shortcomings, many efforts have been made to improve the ferroelectric and piezoelectric properties of SBT ceramics, including: i) A- or B-site substitution, ii) application of low temperature synthesis route, iii) formation of intergrowth structure, iv) using grain orientation techniques, etc. [5–7].

Ashok *et al.* [8] studied Sr doped SBT and measured its T_c = 561 °C, K_p = 59% and d_{33} = 18 pC/N. Wang *et al.* [9] studied Co-doped SBT and found that it had high temperature stability. Zhao *et al.* [10] studied $Na_{0.5}Bi_{4.5}Ti_4O_{15}$–$(x-1)\,Na_{0.5}Bi_{0.5}TiO_3$ and also got the materials with high temperature stability. A-site substitution is more effective than B-site substitution because the cations at B-sites are similar in size and can hardly make a major contribution to the polarization process. Consequently, most reports on enhancing the ferroelectric and piezoelectric properties of SBT ceramics concentrate on A-site rather than B-site modification [11]. It

* Corresponding authors: tel: +86 13659296328,
e-mail: *hldu@foxmail.com*

is found that Ce (A-site substitution) doped in $Bi_4Ti_3O_{12}$ ceramics can appropriately enhance the dielectric and ferroelectric properties [12].

The impedance analysis is the path of studying the grain and grain boundary contribution towards conductivity, and it is a useful method to study the conduction mechanism of the material. Chandra et al. studied the grain and grain boundary contribution towards conductivity of $Ni_{1-x}Mg_xFe_2O_4$ with x = 0.0–1.0 with the Nyquist plots [13]. Naidu *et al.* [14] studied the electrical conduction mechanism with the Cole-Cole plots and the type of relaxation – Debye or non-Debye.

The glycine-nitrate process (GNP) is a low-temperature process with low energy and cost consumption, simple operation and full utilization of energy released between metal nitrate and fuel (glycine). The plate-like SBT ceramics can be synthesized successfully via the glycine-nitrate process under the optimal conditions [15]. Therefore, A-site cerium modified $SrBi_{4-x}Ce_xTi_4O_{15}$ ceramics of x = 0–0.08 were synthesized via the glycine-nitrate process. The dielectric properties (dielectric constant, dielectric loss, temperature coefficient of dielectric constant and the rate of frequency change) were evaluated. Moreover, the conduction mechanism and complex impedance response were analysed by Cole-Cole plots.

II. Experimental

$SrBi_{4-x}Ce_xTi_4O_{15}$ (where x = 0, 0.02, 0.04, 0.06 and 0.08) powders (denoted as SBT-100xCe) were prepared by glycine-nitrate process. Strontium nitrate ($Sr(NO_3)_2$), bismuth nitrate ($Bi(NO_3)_3 \cdot 5H_2O$), butyl titanate ($Ti(OC_4H_9)_4$), cerium nitrate ($Ce(NO_3)_3 \cdot 6H_2O$) and glycine ($C_2H_5NO_2$) were used as starting materials and reaction fuel. Figure 1 shows the detailed flow chart of this experiment.

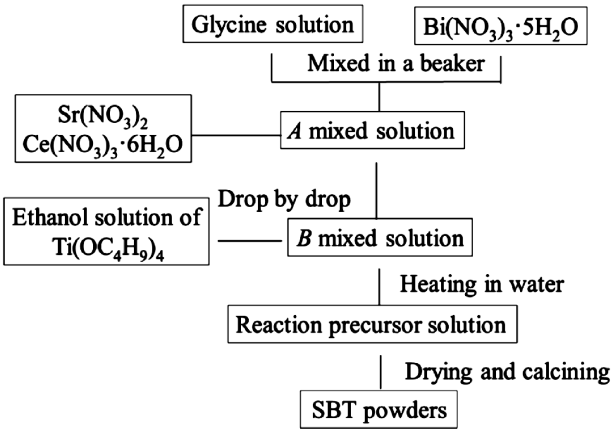

Figure 1. The synthesis process of SBT powder

All raw materials were weighed according to the composition of SBT excluding bismuth nitrate. It was weighed in excess of 2 mol% of the stoichiometric amount to compensate for bismuth volatilization in the high-temperature atmosphere. Then the glycine and nitrates were dissolved into deionized water and $Ti(C_4H_9O)_4$ was dissolved into ethanol. According to the theories of propellant chemistry [16], the amount of glycine (fuel) was calculated for full reaction with nitrates by assuming complete oxidation of the fuel (G/N = 2 : 1). It follows the reaction:

$$Sr(NO_3)_2 + 4\,Bi(NO_3)_3 + 4\,Ti(NO_3)_4 + 18\,C_2H_5NO_2 \rightarrow SrBi_4Ti_4O_{15}\downarrow + 45\,H_2O\uparrow + 36\,CO_2\uparrow + 24\,N_2\uparrow$$

Subsequently, the ethanol solution of butyl titanate was added into the nitrates solution dropwise to obtain a white suspension. It was heated to volatilize ethanol in water bath at 80 °C and formed a uniform and transparent precursor solution, followed by further heating at 100 °C to dehydrate it in order to yield a glycine-nitrate mixture. The resulted mixture was calcined at different temperatures (250, 400, 450 and 500 °C) for up to 2 h to acquire SBT powders.

The calcined powders were mixed with appropriate amount of PVA binder (about 10 wt.%) and then compacted at 20 MPa in a steel die for 1 min to gain pellets with 10 mm diameter and 1–2 mm thickness. Subsequently, the green pellets were placed in program-controlled furnace to continuously burn out PVA and fired at 120, 250 and 550 °C (heating rate: 2 °C/min) for 2 h, respectively. Finally, the green pellet of unmodified SBT was sintered at 1000 °C and the modified ones were sintered at 980 °C for 2 h.

The microstructure of the calcined powders and sintered pellets were investigated by a scanning electron microscope (SEM) (Hitachi S-4800, Japan). The phase identification and structure analysis were performed using X-ray diffractometer (Shimadzu XRD-7000, Japan) with Cu-Kα radiation and 2θ range 10–60°.

In order to measure electrical properties, the ceramic pellets were polished, covered with silver paste and fired at 800 °C for 15 min as electrodes. The temperature and frequency dependence of the dielectric properties of $SrBi_{4-x}Ce_xTi_4O_{15}$ ceramics were measured using a precision LCR meter (Agilent Technologies, Inc. E4980A, USA) with a high temperature dielectric spectrum test system (EMRL XJTU GJW-1, China) in the temperature range of 20–600 °C. The complex impedance (Z^*) measurements as a function of frequency (1 kHz–1 MHz) and temperature (20–700 °C) were carried out using an electrochemical analyser (CH Instruments Inc. CHI660E, USA) with a tube furnace (Carbolite Gero MTF Controller, UK).

III. Results and discussion

3.1. Phase structure and micrograph

The XRD patterns of $SrBi_{4-x}Ce_xTi_4O_{15}$ powders calcined at different temperatures are shown in Fig. 2. The powder heat-treated at 250 °C for 3 h contains $SrTiO_3$, $Bi_4Ti_3O_{12}$ and other unknown phases, which are in accordance with the intermediary products of

redox reactions. It was also shown that the SBT layered-perovskite phases were formed after calcining at 400 °C and the temperature is much lower than with the conventional solid state processes (800–900 °C) [4,17]. Thus, the appropriate conditions for preparation of $SrBi_{4-x}Ce_xTi_4O_{15}$ powders are calcination at 500 °C for 2 h.

A series of the powders was prepared at 500 °C for 2 h and sintered to form bismuth-layered ceramics at 980 °C

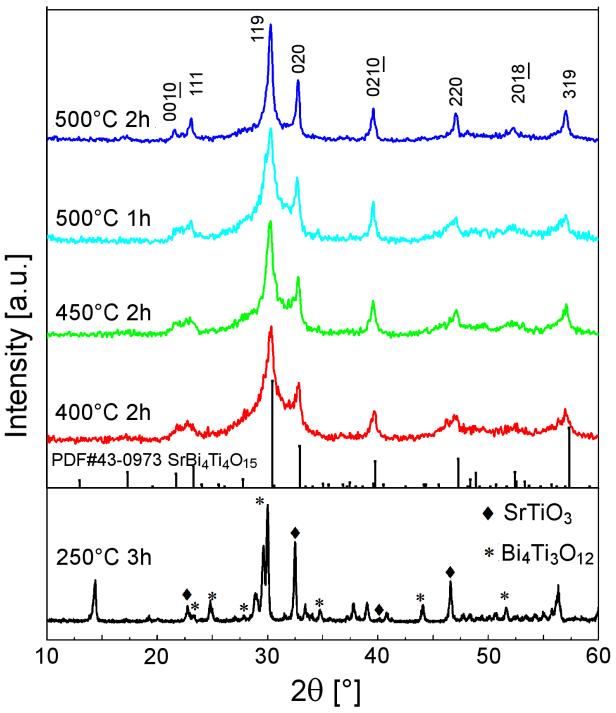

Figure 2. XRD patterns of SBT precursor powders at different temperatures

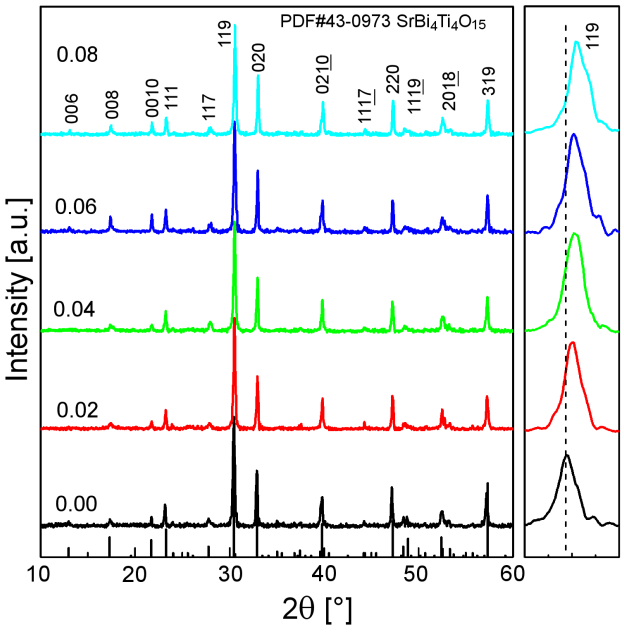

Figure 3. XRD patterns of $SrBi_{4-x}Ce_xTi_4O_{15}$ ceramics with x = 0.00, 0.02, 0.04, 0.06 and 0.08

$SrBi_{4-x}Ce_xTi_4O_{15}$ (x = 0.02, 0.04, 0.06 and 0.08) and 1000 °C ($SrBi_4Ti_4O_{15}$). Figure 3 shows the XRD patterns of $SrBi_{4-x}Ce_xTi_4O_{15}$ ceramics. It can be seen that all patterns are the single SBT phase matched well with standard PDF Card No. 43-0973. This implies that the GNP preparation method decreases the sintering temperature compared to the conventional solid state sintering (1160–1200 °C [18]). XRD results indicate that Ce-doping does not affect the basic crystal structure. It diffuses into the lattice and forms solid solutions. According to the Hume-Rothery rules, it can be ensured that the Bi^{3+} (r = 1.03 Å) is replaced with Ce^{3+} (r = 1.01 Å), since the ratio of ionic radii (1.94%) is much lower than 15%.

Meanwhile, the diffraction peak with the strongest intensity, (119) plane, is in agreement with the principle defined as $11(2m+1)$ observed in BLSFs. The right inset in Fig. 3 shows the enlarged image of the main diffraction 119 peak, which slightly shifts towards the higher angle side with increasing Ce-doping. Thus, according to Bragg equation ($\lambda = 2d \cdot \sin\theta$), the interplanar spacing d decreases, so a slight shrinking of the lattice of the Ce-doped BST is expected. For all ceramic samples, the variations in the lattice parameters and unit cell volume are shown in Fig. 4, which demonstrates that there is a slight reduction in the cell volume. The energy disper-

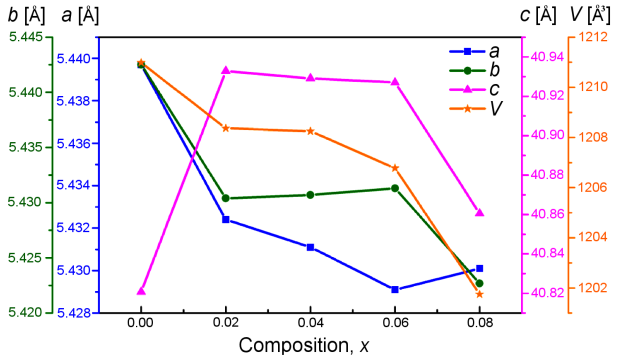

Figure 4. The variations of lattice parameters and volume of $SrBi_{4-x}Ce_xTi_4O_{15}$ with composition (x)

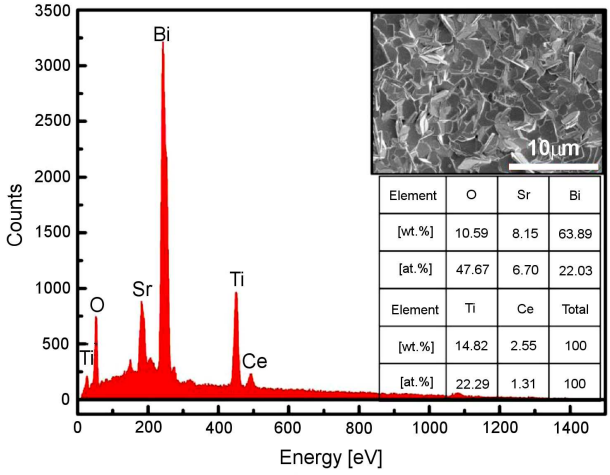

Figure 5. The energy dispersive spectrum of SBT-4Ce

sive spectrum of SBT-4Ce ceramic is shown in Fig. 5. Combined with the XRD and EDS analyses, it is found that the percentage content among different atoms is in the error allowable ranges, and it is generally consistent with the stoichiometry of SBT-4Ce. So, it confirms that Ce ions diffused into the lattice of SBT and partially replaced the Bi^{3+}.

Table 1 shows the change of bulk density of the sintered pellets according to the additive composition. The density of the specimen with proper amounts of Ce was higher measured to be from 7.35 to 7.59 g/cm^3, compared with that of the specimen without Ce (6.83 g/cm^3). This indicated that Ce doped can improve the compactness of the material but excessive addition of Ce can slightly inhibit the densification of BT grains.

Figure 6 presents SEM micrographs of the surface of the sintered $SrBi_{4-x}Ce_xTi_4O_{15}$ ceramics. The ceramics exhibited mostly pallet-shaped dense grains with structural anisotropy and random orientations. Compared with unmodified SBT, it is observed that the grain size of these samples dramatically decreases with increasing x in the composition $SrBi_{4-x}Ce_xTi_4O_{15}$, as well as a more uniform grain size distribution. This indicates that the addition of Ce ions inhibits the grain growth of ceramics because the lattice deformation decreased the interfacial energy to prevent grain boundary diffusion. The size of flake decreases from 12 μm for $x = 0$ to 2 μm for $x = 0.08$, while the thickness varies from around to 0.2 μm. The samples present a high aspect ratio because the grain growth is highly anisotropic on account of the high grain growth rate in the direction perpendicular to the c-axis of the SBT crystal [7], which can be attributed to the increase in the fine grains existing between large anisotropic grains with increasing Ce addition [19].

Table 1. Densities of sintered $SrBi_{4-x}Ce_xTi_4O_{15}$ ceramic samples

Composite	Densities [g/cm^3]
SBT	6.83
SBT-2Ce	7.46
SBT-4Ce	7.59
SBT-6Ce	7.48
SBT-8Ce	7.35

3.2. Analysis of dielectric properties and impedance

The temperature dependence of the dielectric constants (ε_r) and loss ($\tan\delta$) for the sintered $SrBi_{4-x}Ce_xTi_4O_{15}$ ceramics is shown in Fig. 7. The ferroelectric-paraelectric phase transition Curie, temperatures, T_c, for the Ce-doped samples are between 536–542 °C, higher than those (520 °C) reported in literature [20,21] for the pure $SrBi_4Ti_4O_{15}$ ceramics. The small variation (about 20 °C) in T_c is due to the slight lattice distortion because of the small radii difference between of Ce^{3+} and Bi^{3+} [22].

The temperature coefficient of the dielectric constant can be expressed as follows:

$$TCP_{ppm} = \frac{\varepsilon'_{max} - \varepsilon'_{ref}}{\varepsilon'_{ref}\left(T_{max} - T_{ref}\right)} \quad (1)$$

where ε'_{max}, ε'_{ref}, T_{max} and T_{ref} are the maximum dielectric constant in specific temperature range, the dielectric constant at the reference point, the temperature of maximum dielectric constant and the temperature of reference point, respectively. The values of TCP_{ppm}, were calculated in the range from 400 °C to T_c, as shown in Table 2. The temperature stability is better when the value of TCP_{ppm} is decreasing [23].

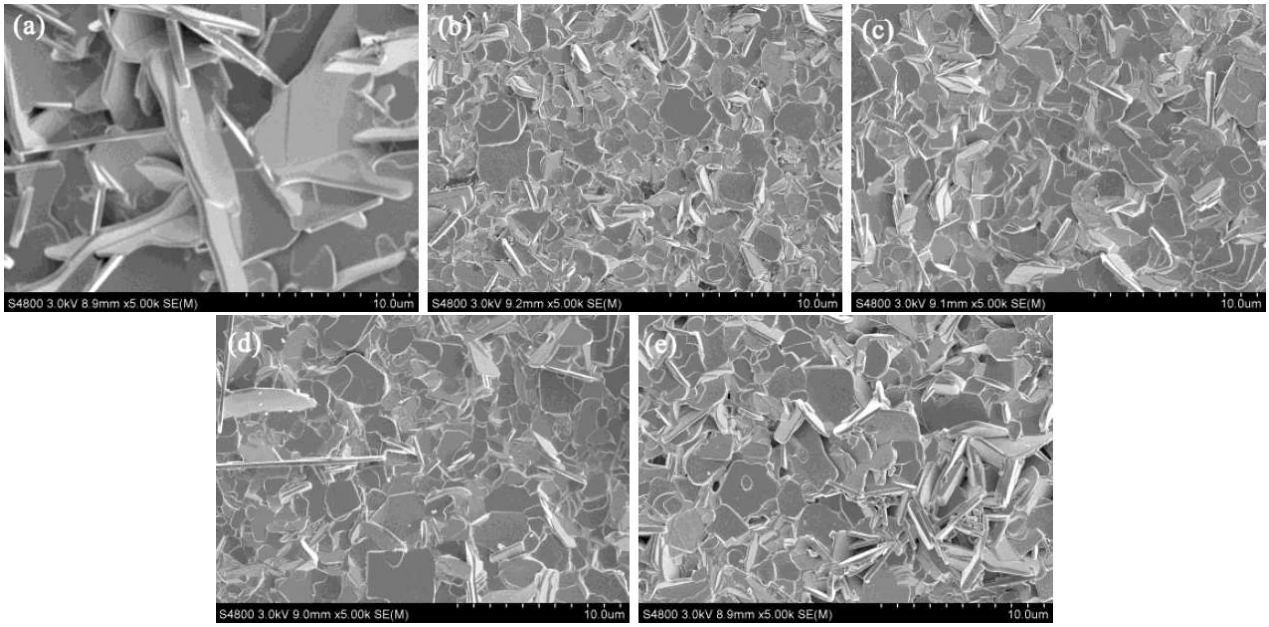

Figure 6. SEM micrographs of the surfaces of $SrBi_{4-x}Ce_xTi_4O_{15}$ ceramics with different Ce-concentration, x: a) 0, b) 0.02, c) 0.04, d) 0.06 and e) 0.08

In addition, ε_r versus temperature curves are broadened and show light relaxor behaviour, which are partially due to the compositional fluctuation in the crystallographic sites and the inhomogeneous distribution of two different cations at the same crystallographic A-site [24]. The phenomenon can be further described by the modified Curie-Weiss law [25]:

$$\ln\left(\frac{1}{\varepsilon'} - \frac{1}{\varepsilon'_m}\right) = \gamma \cdot \ln(T - T_m) + C \qquad (2)$$

where ε'_m is the value of the dielectric constant at T_c and γ ($1 \leq \gamma \leq 2$) is the degree of diffuseness in ferroelectric-paraelectric transition. For normal ferroelectrics, $\gamma = 1$, while for an ideal relaxor, $\gamma = 2$. The insets in Fig. 7 depict the linear fitting and the γ values.

It can be seen that the dielectric constant ε_r decreases with increasing Ce-doping amount at 100 kHz (Fig. 7f), which can be attributed to the degradation of ionic polarization effect because $r(Ce^{3+}) < r(Bi^{3+})$. Also, the Sr^{2+} could be replaced by Ce^{3+}, which would give rise to the electrovalent imbalance leading to the production of A-site vacancies. According to the theory of soft and hard doping, when there are more A-site vacancies, the lattice distortion will be larger and the dielectric constant will decrease. The degradation of the dielectric constant makes it more suitable for tiny electronics like integrated circuits, grid electrodes, etc.

Figure 7f demonstrates that the dielectric losses are below 0.05 from the room temperature to 400 °C,

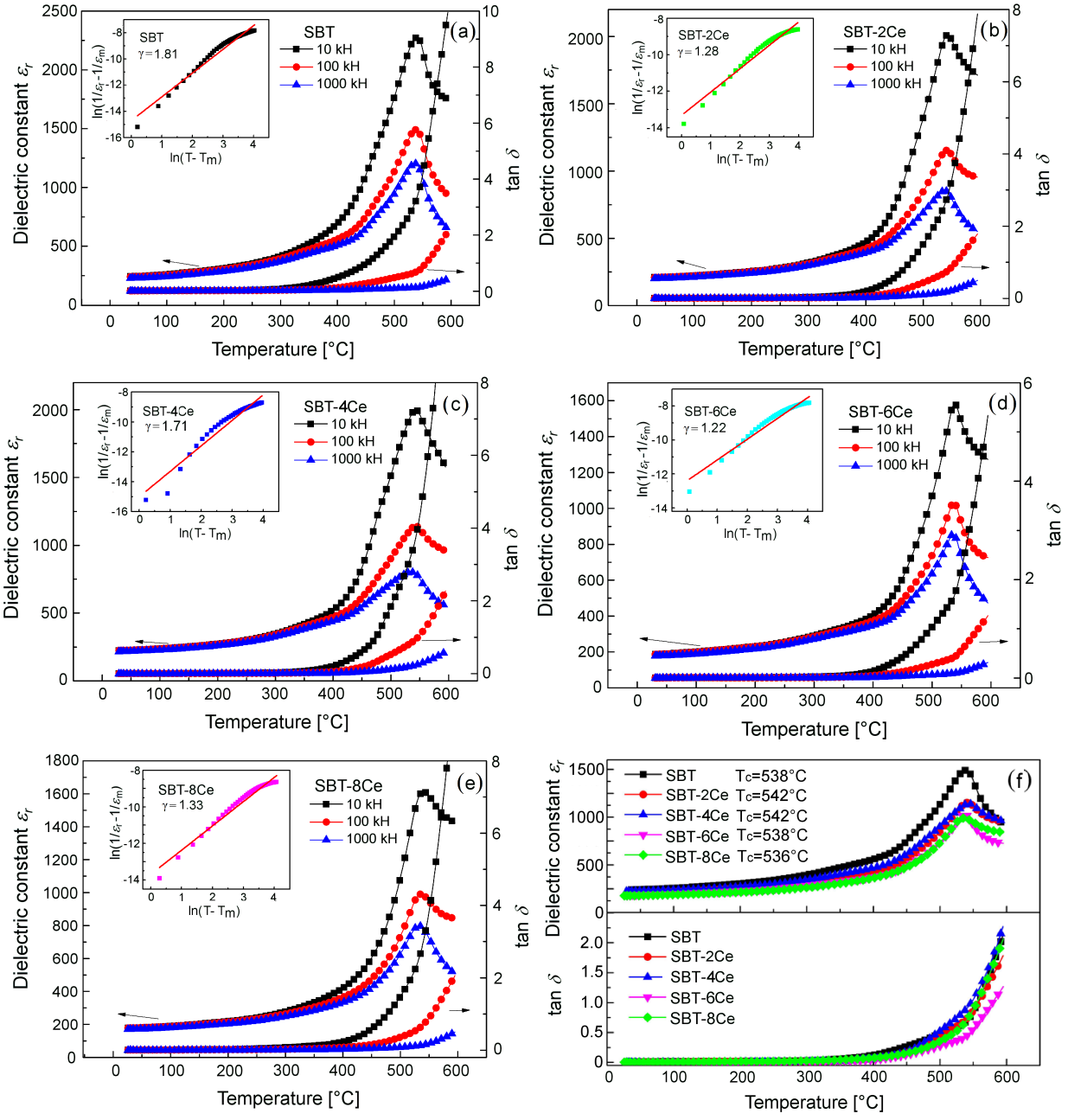

Figure 7. Temperature dependence of the dielectric constant (ε_r) and dielectric loss ($\tan\delta$) of $SrBi_{4-x}Ce_xTi_4O_{15}$ ceramics with different Ce-concentration, x: a) 0, b) 0.02, c) 0.04, d) 0.06, e) 0.08 and f) the dielectric properties for all samples at 100 kHz

Table 2. Dielectric parameters of sintered $SrBi_{4-x}Ce_xTi_4O_{15}$ ceramic samples at 100 kHz

Composition	ε_r at 35 °C	tan δ at 35 °C	tan δ at 400 °C	T_c [°C]	ε'_m	γ	TCP_{ppm}	η
SBT	241	0.0049	0.0378	538	1491	1.81	0.0121	0.0428
SBT-2Ce	209	0.0031	0.0438	542	1154	1.28	0.0122	0.0190
SBT-4Ce	224	0.0004	0.0535	542	1140	1.71	0.0101	0.0033
SBT-6Ce	186	0.0033	0.0434	538	1030	1.22	0.0128	0.0182
SBT-8Ce	179	0.0045	0.0756	536	991	1.33	0.0127	0.0350

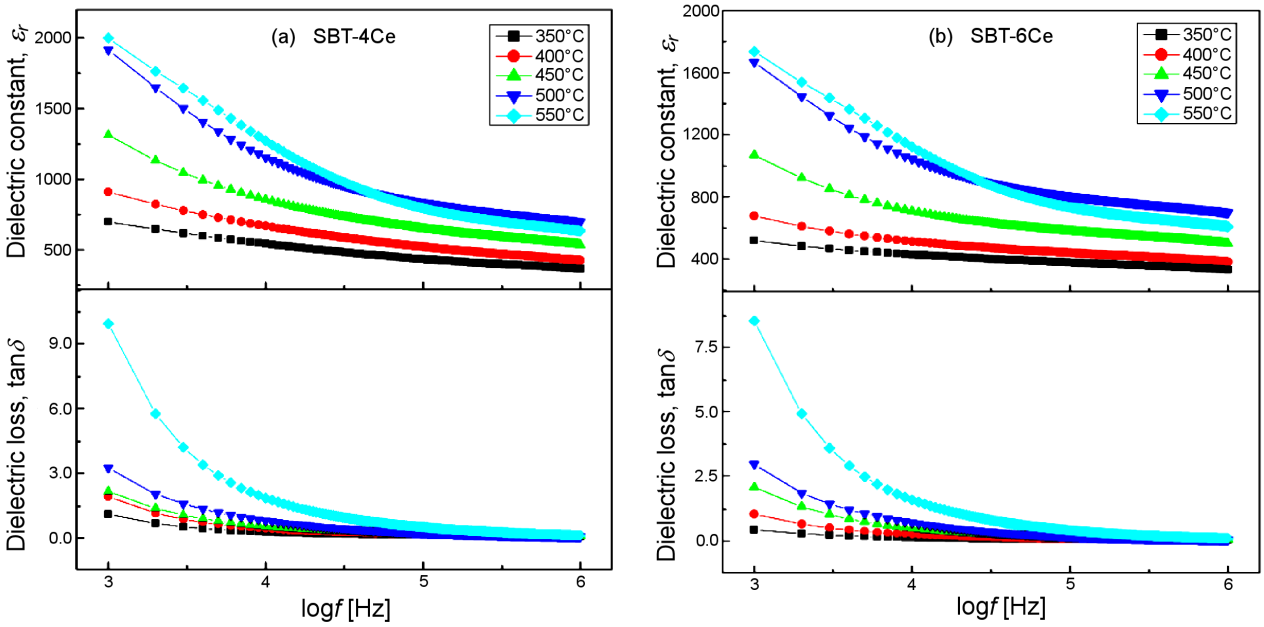

Figure 8. The frequency dependence of the dielectric constant ε' and dielectric loss tan δ as a function of temperature for $SrBi_{4-x}Ce_xTi_4O_{15}$ ceramics: a) x = 0.04 and b) x = 0.06

which shows that the $SrBi_{4-x}Ce_xTi_4O_{15}$ ceramics possess highly stable dielectric properties. The small loss can be explained by the substitution of Bi^{3+} by Ce^{3+}, which degrades the concentrations of oxygen vacancies and electrons originating from the Bi_2O_3 volatilization, which inhibits the motion of these free charge carriers, leading to the decreased dielectric losses [26]. However, the value of the tan δ rises sharply above T_c for all doping concentrations. That may stem from the space charge polarization and the conductivity beginning to dominate above T_c. The values for the ε_r at 35 °C, maximum ε_m, tan δ at 35 °C and tan δ at 400 °C, as well as T_c of the $SrBi_{4-x}Ce_xTi_4O_{15}$ ceramics are shown in Table 2.

Figure 8 shows the frequency dependence of ε_r and tan δ for $SrBi_{4-x}Ce_xTi_4O_{15}$ with x = 0.04, 0.06. It can be seen that SBT ceramics show stable permittivities and small dielectric loss at the temperature range of 350–450 °C, giving rise to the frequency stability. In the entire temperature range, ε_r and tan δ have similar variation trends and relative stability, which indicates that there is little frequency dependence of the sintered ceramics. Also, the frequency stability can be measured by using the rate of frequency change (η) and it is defined as:

$$\eta = \frac{\varepsilon'(f_0) - \varepsilon'(f)}{\varepsilon'(f_0)} \tag{3}$$

where $\varepsilon'(f_0)$ and $\varepsilon'(f)$ are the dielectric constant at 100 Hz and measured frequency f, respectively. The values of η, calculated in the condition of 100 kHz and 40 °C, are shown in Table 2.

Generally, the carriers migrate along the path through the grains and grain boundaries, inducing Maxwell-Wagner polarization. That will produce resistance and capacitance in the grain and grain boundary, so the main conduction mechanism is related to the responses of grain and grain boundary for most ceramics. Figure 9 shows the equivalent circuit used for the Ce-doped SBT ceramics. Figure 10 shows the temperature dependence of the complex impedance spectra (Cole-Cole plots) for $SrBi_{4-x}Ce_xTi_4O_{15}$ (x = 0, 0.02, 0.04, 0.06 and 0.08) and the insets are the enlarged local images. Along with frequency increase, the Ce-doped $SrBi_4Ti_4O_{15}$ system

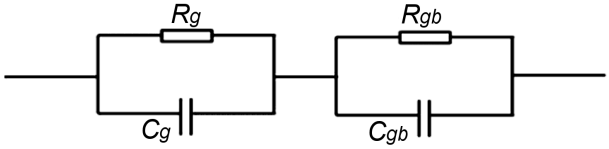

Figure 9. The equivalent circuit diagram

undergoes various relaxations: space charges relax at lower frequencies, the grain boundary relaxation in the middle while the grain relaxation occurs at higher frequencies [27]. In this connection Cole-Cole plots were drawn (Fig. 10) for complex impedance between Z' and Z'' at various temperatures. At room temperature, there is no semiconductor behaviour. Although data points represent semicircles, the relaxations are of non-Debye type since the centres of semicircles lie below the real axis of the impedance.

On the other hand, at elevated temperatures all compositions exhibit complete semicircle arcs. The centres

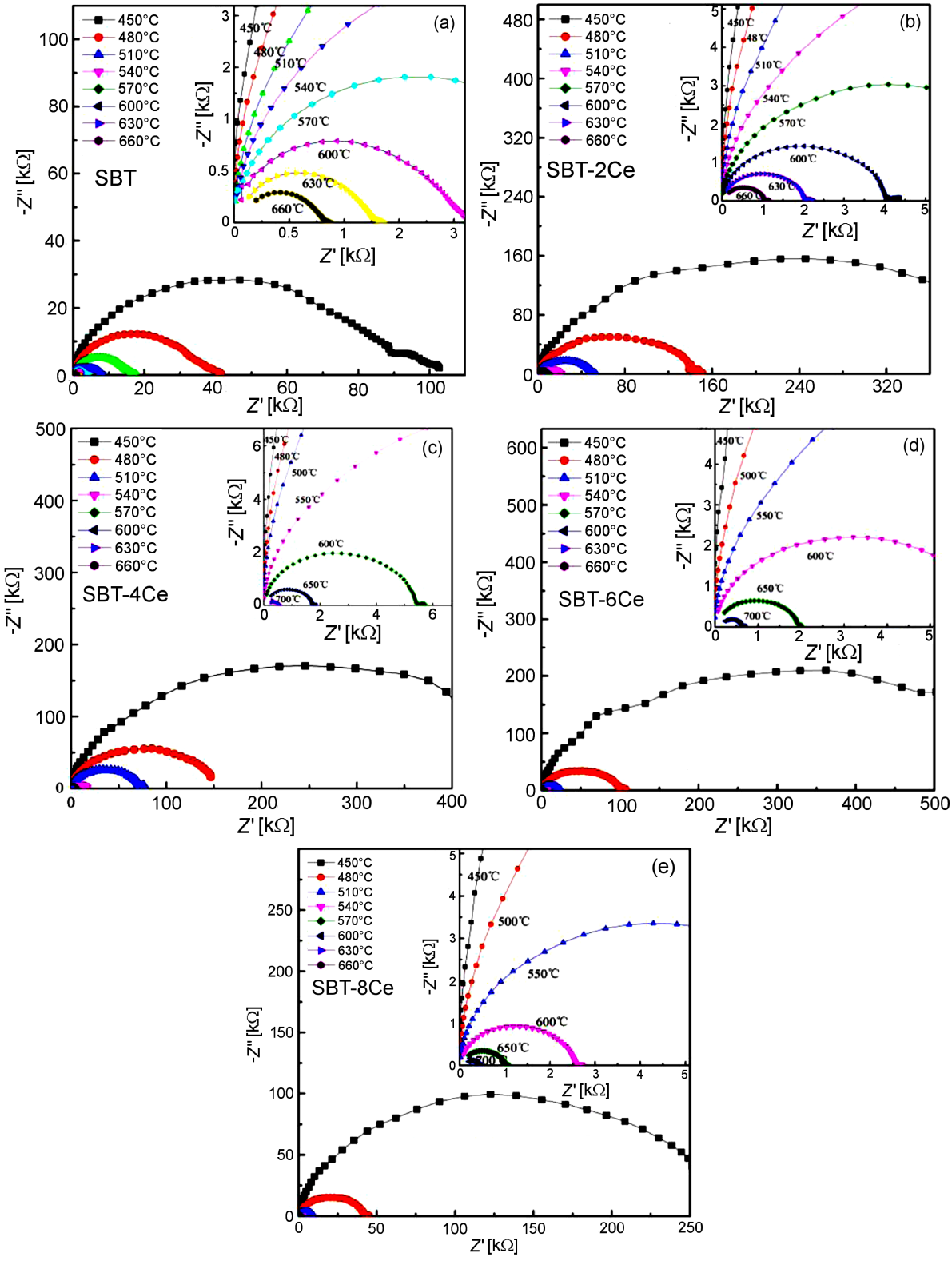

Figure 10. The complex impedance plots for $SrBi_{4-x}Ce_xTi_4O_{15}$ ceramics with different Ce-concentration, x: a) 0, b) 0.02, c) 0.04, d) 0.06 and e) 0.08

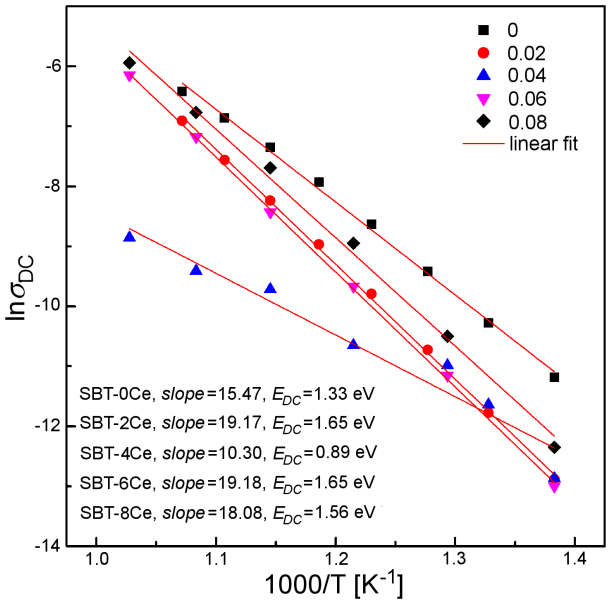

Figure 11. The Arrhenius plots of $\ln \sigma_{DC}$ vs. $1000/T$ for $SrBi_{4-x}Ce_xTi_4O_{15}$ ceramics with different Ce-doping

of these arcs are above real axis and hence it is confirmed that the present samples are of higher homogeneity and obey ideal Debye relaxation [28]. It is indicated that the conduction mechanism is not affected by the Ce doping, and the arc is smaller when the temperature is higher. This phenomenon illustrates that the loss becomes heavier and induces the degradation of impedance. The low frequency semicircle and the high frequency semicircle can be attributed to the grain boundary and the grain, respectively, because the capacitance and resistance of the grain boundary are higher [29]. In addition, the Ce-doped samples have larger impedance values, which are much larger than the unmodified value of 100 kΩ at 450 °C. When $x = 0.06$, the impedance value rises to the maximum at about 600 kΩ. It can be explained that the loss is reduced when Ce ions are doped into the lattice of SBT according to the analysis of dielectric properties results. When $x = 0.08$, the increased loss indicates the reduction of impedance value because of the lattice distortion. From the insets in Fig. 10, it can be observed that the intersection of semicircle with x-axis does not equal zero for all compositions at high frequencies, owing to the restriction of measurement frequency in this experiment. In fact, there could be a fainter arc, which coincides with the phenomenon occurred in the research of the layered $CaCu_3Ti_4O_{12}$ and can be ascribed to the response of domain boundary [30].

According to the complex impedance (Cole-Cole) plots, the DC conductivity and activation energy resulting from the defect and vacancy can be evaluated [5]. The intercept of the semicircular arc on real axis gives the total resistance (R_{tot}), and the DC conductivity (σ_{DC}) of the bulk can be calculated using the relation:

$$\sigma_{DC} = \frac{t}{R_{tot} \cdot S} \tag{4}$$

where S and t are the electrode surface area and thickness of the pellet, respectively. The activation energy (E_{DC}) for the DC conductivity can be obtained from the Arrhenius equation (Eq. 5), using the slope in the plot of $\ln \sigma_{DC}$ versus $1000/T$. Typical conductivity dependence on the temperature is shown in Fig. 11, where it is noticed that the conductivity gradually increases with increasing temperature.

$$\sigma_{DC} = \sigma_0 \cdot \exp\left(-\frac{E_{DC}}{k_B \cdot T}\right) \tag{5}$$

The activation energy E_{DC}, calculated for all compositions, is obviously different which may be due to the effect of material defects on the activation energy. Because of the lattice distortion, the E_{DC} of SBT-4Ce is the lowest.

Variations in the real and imaginary parts (Z', Z'') of impedance with frequency at different temperatures are illustrated in Fig. 12. From Fig. 12a, it can be easily noticed that the value of Z' declines with the increase in both temperature and frequency. The Z' values of all samples gradually converge at selected temperatures when the frequency is over 100 kHz. It is indicated that the impedance of grains and grain boundaries are re-

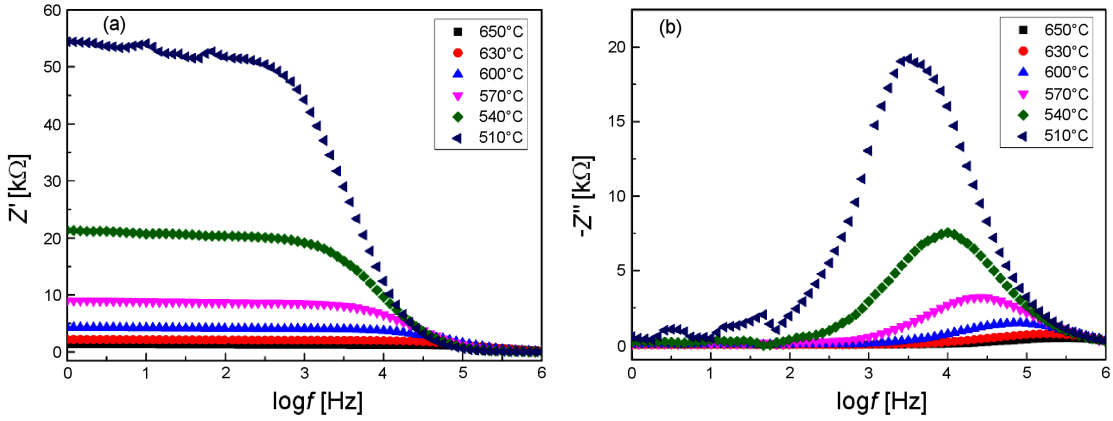

Figure 12. The impedance as a function of frequency for SBT-4Ce ceramics at selected temperatures: a) real and b) imaginary part

duced, and there is electrode interface resistance, which releases the space charges [31]. However, the values of Z'' for all temperatures go through a period of ups and downs with increasing frequency, which are given in Fig. 12b. As the temperature and frequency rise, the value of Z'' reduces and eventually merges into the high frequency domain. So, the presence of space charge polarization effects is at lower frequencies and higher temperatures [8]. The multiple relaxations may be due to the presence of free electrons at lower temperatures and structural changes as defects and/or vacancies at higher temperatures [32].

IV. Conclusions

The $SrBi_{4-x}Ce_xTi_4O_{15}$ (where x = 0, 0.02, 0.04, 0.06 and 0.08) samples were successfully prepared by glycine-nitrate process and sintering. The structure, phase, dielectric properties and impedance were investigated. The obtained results show that the SBT powders can be obtained by GNP at 400 °C, which is lower than the traditional solid-state reaction temperature of 800–900 °C. XRD and EDS confirm the formation of a single phase and that Bi is replaced by Ce in the SBT structure, which induces a small reduction in unit cell volume. The SEM reveals that the plate-like morphology has a high aspect ratio and the grain size is dramatically decreased compared with unmodified SBT. That indicates that the addition of Ce ions inhibits the grain growth of ceramics. The T_c slightly fluctuated (20 °C) due to the mildly distorted lattice resulting from Ce doping. The introduction of Ce can reduce dielectric losses which are below 0.05 up to 400 °C. The TCP_{ppm} is only about 0.012 and η is 0.01–0.04, which indicates that $SrBi_{4-x}Ce_xTi_4O_{15}$ ceramics possess highly stable dielectric properties. Impedance analysis reveals that the conduction mechanism of the $SrBi_{4-x}Ce_xTi_4O_{15}$ ceramics is mainly grain conduction. The high resistance of Ce-doped ceramics can induce the small leakage current. The variation in Z' can induce a reduction in the impedance of grains, grain boundaries, electrode interface and the release of space charges. The shift of Z'' shows that there are space charges which depend on the frequency and temperature.

Acknowledgement: This work was supported by the National Natural Science Foundation of China under Grant number 51372197; Major International Joint Research Program of Shaanxi Province under Grant number 2012KW-10; and Key Innovation Team of Shaanxi Province under Grant number 2014KCT-04.

References

1. B.H. Park, B.S. Kang, S.D. Bu, T.W. Noh, J. Lee, W Jo., "Lanthanum-substituted bismuth titanate for use in non-volatile memories", *Nature*, **401** [6754] (1999) 682–684.
2. B. Aurivillius, "Mixed bismuth oxide with layer lattices II Structure of $Bi_4Ti_3O_{12}$", *Arkiv. Kemi.*, **1** (1949) 499–512.
3. E.V. Ramana, M.P.F. Graça, M.A. Valente, T.B. Sankaram, "Improved ferroelectric and pyroelectric properties of Pb-doped $SrBi_4Ti_4O_{15}$ ceramics for high temperature applications", *J. Alloys. Compd.*, **583** (2014) 198–205.
4. P. Nayak, T. Badapanda, S. Panigrahi, "Dielectric, ferroelectric and conduction behavior of tungsten modified $SrBi_4Ti_4O_{15}$ ceramic", *J. Mater. Sci. Mater. Electron.*, **27** [2] (2016) 1217–1226.
5. G. Parida, J. Bera, "Electrical properties of niobium doped $Bi_4Ti_3O_{12}$-$SrBi_4Ti_4O_{15}$ intergrowth ferroelectrics", *Ceram. Int.*, **40** [2] (2014) 3139–3144.
6. P. Ferrer, J.E. Iglesias, A. Castro, "Synthesis of the Aurivillius phase $SrBi_4Ti_4O_{15}$ by a mechanochemical activation route", *Chem. Mater.*, **16** [7] (2004) 1323–1329.
7. H.B. Chen, B. Shen, J.B. Xu, J.W. Zhai, "Textured $Ca_{0.85}(Li,Ce)_{0.15}Bi_4Ti_4O_{15}$ ceramics for high temperature piezoelectric applications", *Mater. Res. Bull.*, **47** [9] (2012) 2530–2534.
8. K. Ashok, B. Mamatha, P. Sarah, "Electrical properties of lead free $Sr_{0.8}Na_{0.1}Sm_{0.1}Bi_4Ti_4O_{15}$ ceramics", *Proced. Mater. Sci.*, **10** (2015) 542–547.
9. Q. Wang, Z.P. Cao, C.M. Wang, Q.W. Fu, D.F. Yin, H.H. Tian, "Thermal stabilities of electromechanical properties in cobalt-modified strontium bismuth titanate ($SrBi_4Ti_4O_{15}$)", *J. Alloys Compd.*, **674** (2016) 37–43.
10. M.L. Zhao, Q.Z. Wu, C.L. Wang, J.L. Zhang, Z.G. Gai, C.M. Wang, "Dielectric and piezoelectric properties of $Na_{0.5}Bi_{4.5}Ti_4O_{15}$–(x-1)$Na_{0.5}Bi_{0.5}TiO_3$ composite ceramics", *J. Alloys Compd.*, **476** [1-2] (2009) 393–396.
11. T.L. Zhao, C.M. Wang, C.L. Wang, Y.M. Wang, S. Dong, "Enhanced piezoelectric properties and excellent thermal stabilities ofcobalt-modified Aurivillius-type calcium bismuth titanate ($CaBi_4Ti_4O_{15}$)", *Mater. Sci. Eng. B*, **201** (2015) 51–56.
12. C.M. Wang, L. Zhao, J.F. Wang, L.M. Zheng, J. Du, M.L. Zhao, C.L. Wang, "Cerium-modified Aurivillius-type sodium lanthanum bismuth titanate with enhanced piezoactivities", *Mater. Sci. Eng. B*, **163** (2009) 179–183.
13. K.C.B. Naidu, S. Roopas Kiran, W. Madhuri, "Investigations on transport, impedance and electromagnetic interference shielding properties of microwave processed NiMg ferrites", *Mater. Res. Bull.*, **89** (2017) 125–138.
14. K.C.B. Naidu, W. Madhuri, "Hydrothermal synthesis of $NiFe_2O_4$ nano-particles: structural, morphological, optical, electrical and magnetic properties", *Bull. Mater. Sci.*, **40** [2] (2017) 417–425.
15. C.S. Naveen, M.L. Dinesha, H.S. Javanna, "Effect of fuel to oxidant molar ratio on structural and dc electrical conductivity of ZnO nanoparticles prepared by simple solution combustion method", *J. Mater. Sci. Technol.*, **29** [10] (2013) 898–902.
16. F.R. Sale, F. Mahloojchi, "Citrate gel processing of oxide superconductor", *Ceram. Int.*, **14** [4] (1998) 229–237.
17. A.R. James, "Effect of oxygen assisted sintering on piezoelectric properties of $SrBi_4Ti_4O_{15}$ ceramics prepared via high energy mechanochemical processing", *Ceram. Int.*, **41** [3] (2015) 5100–5106.
18. P. Sarah, "Electric properties of holmium substituted $SrBi_4Ti_4O_{15}$ ceramic for high temperature piezoelectric applications", *Procedia. Eng.*, **10** [7] (2011) 2684–2689.
19. Q.Y. Tang, Y.M. Kan, Y.G. Li, G.J. Zhang, P.L. Wang, "Effect of vanadium doping on fabrication and property of $Bi_4Ti_3O_{12}$ ceramics", *Scr. Mater.*, **54** [12] (2006) 2075–

2080.
20. L.Y. Zheng, G.R. Li, Q.R. Yin, K.W. Kwok, "Phase transition and failure at high temperature of bismuth-layered piezoelectric ceramics", *J. Am. Ceram. Soc.*, **89** [4] (2006) 1317–1320.
21. Z.J. Xu, R.Q. Chu, J.L. Hao, Q.R. Yin, "A novel hybrid method of sol-gel and ultrasonic atomization synthesis and piezoelectric properties of $SrBi_4Ti_4O_{15}$ ceramics", *J. Am. Ceram. Soc.*, **91** [3] (2008) 910–913.
22. O. Subohi, R. Singh, G.S. Kumar, M.M. Malik, R. Kurchania, "Impedance analysis and dielectric properties of Ce modified bismuth titanate lead free ceramics synthesized using solution combustion route", *J. Mater. Sci. Mater. Electron.*, **26** [11] (2015) 1–12.
23. R.H. Liang, X.L. Dong, Y. Chen, F. Cao, Y.L. Wang, "Effect of ZrO_2 doping on the tunable and dielectric properties of $Ba_{0.55}Sr_{0.45}TiO_3$/MgO composites for microwave tunable application", *Mater. Res. Bull.*, **41** [7] (2006) 1295–1302.
24. G. Parida, J. Bera, "Effect of La-substitution on the structure, dielectric and ferroelectric properties of Nb modified $SrBi_8Ti_7O_{27}$ ceramics", *Mater. Res. Bull.*, **68** (2015) 155–159.
25. C.L. Diao, J.B. Xu, H.W. Zheng, L. Fang, Y.Z. Gu, W.F. Zhang, "Dielectric and piezoelectric properties of cerium modified $BaBi_4Ti_4O_{15}$ ceramics", *Ceram. Int.*, **39** [6] (2013) 6991–6995.
26. L.J. Fei, Z.Y. Zhou, S.P. Hui, X.L. Dong, "Effects of La^{3+} substitution on structure and temperature dependence of electrical properties of $CaBi_4Ti_4O_{15}$-$Bi_4Ti_3O_{12}$ ceramics", *J. Mater. Sci. Mater. Electron.*, **26** [9] (2015) 6843–6847.
27. K.C.B. Naidu, W. Madhuri, "Microwave assisted solid state reaction method: investigations on electrical and magnetic properties of NiMgZn ferrites", *Mater. Chem. Phys.*, **181** (2016) 432–443.
28. Z.V. Mocanu, M. Airimioaei, C.E. Ciomaga, L. Curecheriu, F. Tudorache, S. Tascu, A.R. Iordan, N.N.M. Palamaru, L. Mitoseriu, "Investigation of the functional properties of $Mg_xNi_{1-x}Fe_2O_4$ ceramics", *J. Mater. Sci.*, **49** (2014) 3276–3286.
29. Ch. Sameera Devi, M.B. Suresh, G.S. Kumar, G. Prasad, "Synthesis, characterization and electrical properties of Nd/Zr co-doped nano $BaTiO_3$ ceramics", *J. Adv. Dielectr.*, **2** [1] (2012) 1250001.
30. T.T. Fang, C.P. Liu, "Evidence of the internal domains for inducing the anomalously high dielectric constant of $CaCu_3Ti_4O_{12}$", *Chem. Mater.*, **17** [20] (2005) 5167–5171.
31. T. Badapanda, V. Senthil, S.K. Rout, S. Panigrahi, T.P. Sinha, "Dielectric relaxation on $Ba_{1-x}Bi_{2x/3}Zr_{0.25}Ti_{0.75}O_3$ ceramic", *Mater. Chem. Phys.*, **133** [2-3] (2012) 863–870.
32. G.S. Lotey, N.K. Verma, "Structural, magnetic, and electrical properties of Gd-doped $BiFeO_3$ nanoparticles with reduced particle size", *J. Nanopart. Res.*, **14** [3] (2012) 742.